https://doi.org/10.1016/j.ymssp.2020.107187
This is the Pre-Published Version.

Active Disturbance Rejection Control of Test Sample in Electrostatic Suspension System

Biao Xiang[1], Qingyuan Guo[2] and Waion Wong[1]

1 Department of Mechanical Engineering, The Hong Kong Polytechnic University, Hung Hom, Kowloon, Hong Kong SAR, China

2 Key Laboratory of Space Utilization, Technology and Engineering Center for Space Utilization, Chinese Academy of Sciences, No.9 Dengzhuang South Road, Haidian District, Beijing, China

***Abstract*:** The electrostatic suspension system is a contactless detective method to analyze the material properties of test sample. In this article, the characteristics about electric field force and electric image force of an electrostatic suspension system are analyzed, and the force analysis and dynamic functions of test sample in the electrostatic suspension system are developed. The suspension precision of test sample in vertical direction is sensitive to the gravity and the disturbances. Therefore, an active disturbance rejection control (ADRC) model including a displacement control loop and an acceleration control loop is designed to the suspension control of test sample. The simulation and experiment are conducted to validate the effectiveness of ADRC model when the random and impulse disturbances are imposed on the test sample in vertical direction, and results indicate that the ADRC model could improve the robust stability of test sample and reduce the oscillation amplitude of high voltage electrodes.

***Keywords*:** electrostatic suspension system; electric field force; high voltage electrode; active disturbance rejection control.

1 Introduction

The electrostatic suspension system is used as a contactless detective technique of material testing by suspending the detected sample at the equilibrium position [1, 2]. This technology is widely applied to the researches about the undercooling materials [3, 4], the metastable materials [4, 5] and other new functional materials [6-8] by avoiding the contact between the test sample and the container, and it could effectively restrain the heterogeneous nucleation. Compared to other suspension methods such as the electromagnetic suspension system [9, 10], the aerodynamic suspension system [11] and the acoustic suspension system [12], the electrostatic suspension system could suspend the nonmetallic materials, realize the suspension in vacuum environment and separate the heating from the suspension. More importantly, the electrostatic suspension system causes little influence on the test sample with better control performance [13].

For suspension control of test sample in the electrostatic suspension system on the ground, the electrostatic suspension system must generate the electric filed force to overcome the gravity of test sample in vertical direction [14], so the stabilization control of test sample in the electrostatic suspension system is an important research topic. Firstly, in order to generate enough electric field force to overcome the gravity, the test sample should have a large amount of charges in the high voltage (HV) electrodes with a short airgap [15]. Therefore, the stabilization control of test sample in the electrostatic suspension system should have quick response speed to make the test sample stably suspends from the initial unstable position to the equilibrium position. Moreover, the high steady-state suspension precision is required to ensure the precise measurement about test sample in the electrostatic suspension system. Furthermore, because the initial charged state of test

© 2020. This manuscript version is made available under the CC-BY-NC-ND 4.0 license http://creativecommons.org/licenses/by-nc-nd/4.0/

sample is complex and the charge of test sample would be declined during the heating and molten process, the stabilization control system of test sample in the electrostatic suspension system should have strong ability on disturbance rejection.

In order to improve the stability and control precision of test sample in the electrostatic suspension system, a time-delay controller was designed [16, 17], and the bias voltage of electrostatic suspension system was derived based on the maximum acceptable time-delay. A single-axis feedback control scheme was proposed to realize the quick response of test sample in the electrostatic suspension system [18], and the experimental results showed that the control model has satisfactory levitation stability in both upright and horizontal directions. Based on the approximated linear model of electrostatic suspension system in [19], a gain-scheduling control was used to the position control of electrostatically levitated material, and the charge of levitated material is estimated by a discrete-time extended Kalman filter. Finally, experimental results verified that the gain-scheduled control achieved a better performance than the fixed-gain control model. A simple fuzzy logic scheme for online tuning parameters of proportional integral (PI) control model was studied in the wheel-like rotor levitated by electrostatic force to improve the robustness [20], the overshoot was reduced to 17% compared with 27% of the conventional PI controller, and the rise time for two control channels was 3.6ms and the settle time was nearly 25.6ms, so the results presented a quick response time and good steady-state performance.

Although the stabilization control of test sample in the electrostatic suspension system had been realized in those above-mentioned papers, the disturbance influence and the variable electric image force in the electrostatic suspension system were not analyzed and suppressed. Therefore, this article will study the dynamic models of test sample in the electrostatic suspension system with different disturbances and the electric image force. Considering the anti-disturbance performance of the active disturbance rejection control (ADRC) [21-24], an ADRC model including a displacement control loop and an acceleration control loop is designed to suppress the disturbance acting on test sample in the electrostatic suspension system. The major contributions of this article include:

1, analyze the influence caused by the electric image force, and the stable suspension conditions of test sample in the electrostatic suspension system are proposed.

2, develop the dynamic model of test sample in electrostatic suspension system with electric image force.

3, an ADRC model with a displacement control loop and an acceleration control loop is designed to improve suspension precision of test sample in electrostatic suspension system.

This article is organized as follows. The structure of an electrostatic suspension system is introduced in section 2. Furthermore, the ADRC model is designed for the electrostatic suspension system in section 3. The numerical simulations are performed to verify the anti-disturbance ability of electrostatic suspension system with the ADRC model in section 4. The experiments are conducted to evaluate the control performances of test sample in the electrostatic suspension system in section 5. Finally, some conclusions are summarized.

2 Model of Electrostatic Suspension System

2.1 Prototype of Electrostatic Suspension System

The prototype of electrostatic suspension system is shown in Fig. 1(a), three pairs of HV electrodes in the sealed container control the stable suspensions of test sample on six degrees of freedom (DOFs) based on the displacement feedback. The simplified model of test sample on *xy* plane and the control loop of electrostatic suspension system are illustrated in Fig. 1(b). The whole electrostatic suspension system has five sub-systems including the actuator system, the measurement system, the main control unit (MCU), the high voltage amplifier (HVA) system and the high voltage power supply (HVPS) system. The actuator system has three pairs of HV electrodes along *x*, *y* and *z* axes, and they generate electric field forces to suspend the test sample at vertical and horizontal equilibrium positions. The measurement system is consisted of two orthogonal binocular vision cameras, and the light sources are applied to make the test sample generates shadow to the camera during heating test sample, so the displacements of test sample along vertical and horizontal directions could be measured. Simultaneously, the light sources also replenish the charge of test sample, and their fixation heights are same as the HV electrodes on *xy* plane. The MCU system based on multi-core graphic processing unit (GPU) and Soc chip could realize the image processing of test sample and the programming of ADRC model. The digital-analog (DA) unit converts the digital signal to the analogy signal, and then the control voltages for three pairs of HV electrodes are generated through the HVAs in different control channels. Finally, three HV electrodes generate the electric field forces to control the stable suspension of test sample through the HVPS system.

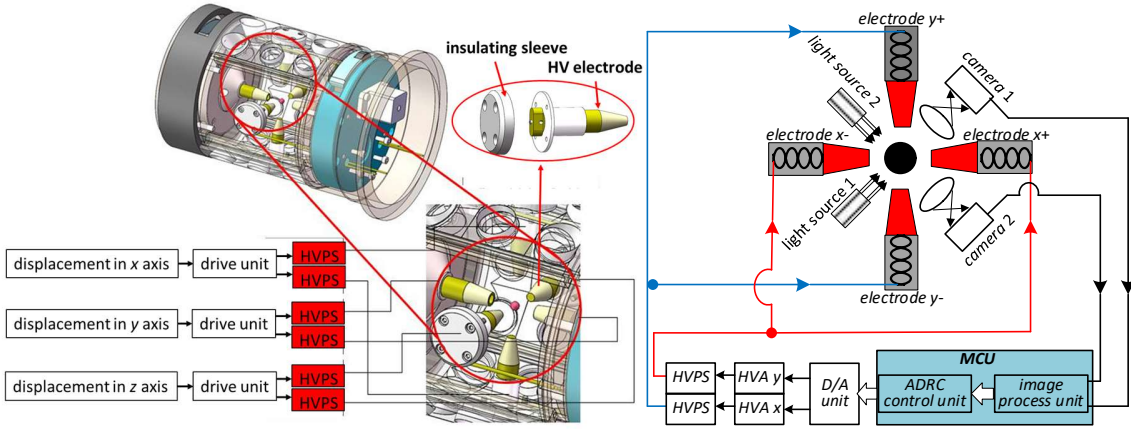

(a) (b)

Fig. 1. (a) The prototype of electrostatic suspension system, (b) the simplified model of electrostatic suspension system.

2.2 Model of Test Sample with HV Electrode

As shown in Fig. 2(a), the test sample is suffering the electric field force f_{ez}, the electric image force f_{iz} and the gravity mg in vertical direction. U_z is the control voltage between the top electrode z+ and the below electrode z- in vertical direction, d is the vertical airgap between the top electrode z+ and the below electrode z-, and d_z is the vertical airgap between the center of test sample and the below electrode z-.

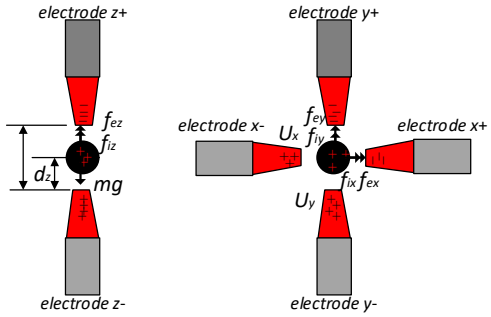

(a) (b)

Fig. 2. Force model of test sample in HV electrodes, (a) force analysis of test sample in vertical direction, (b) force analysis of test sample in horizontal direction.

In order to make the test sample stably suspended at the equilibrium position in vertical direction, the electric field force satisfies the condition as following

$$f_{ez} \geq f_{iz} + mg \tag{1}$$

The electric field force is expressed into

$$f_{ez} = Q_s \frac{U_z}{d_z} \tag{2}$$

The electric image force is

$$f_{iz} = \frac{Q_s^2}{16\pi\varepsilon_0}\left[\frac{1}{(d_{zn} - d_z)^2} - \frac{1}{d_z^2}\right] \tag{3}$$

where Q_s is the charge of test sample, and ε_0 is the permittivity of vacuum.

As illustrated in Fig. 2(b), the electric field forces acting on the test sample in horizontal direction could be respectively written into

$$\begin{cases} f_{ex} = Q_s \dfrac{U_x}{d_x} \\ f_{ey} = Q_s \dfrac{U_y}{d_y} \end{cases} \tag{4}$$

And the electric image forces in horizontal direction are respectively expressed into

$$\begin{cases} f_{ix} = \dfrac{Q_s^2}{16\pi\varepsilon_0}\left[\dfrac{1}{(d_{yn} - d_y)^2} - \dfrac{1}{d_y^2}\right] \\ f_{iy} = \dfrac{Q_s^2}{16\pi\varepsilon_0}\left[\dfrac{1}{(d_{xn} - d_x)^2} - \dfrac{1}{d_x^2}\right] \end{cases} \tag{5}$$

In horizontal direction, the airgap between the positive electrode and the negative electrode is quite large, and the test sample is always suspended at the equilibrium position without considering the influence of gravity. Therefore, the electric field force is far greater than the electric image force in horizontal direction, and the relationship between electric field force and electric image force is expressed as following

$$\begin{cases} Q_s \dfrac{U_y}{d_y} \gg \dfrac{Q_s^2}{16\pi\varepsilon_0}\left[\dfrac{1}{(d_{yn} - d_y)^2} - \dfrac{1}{d_y^2}\right] \\ Q_s \dfrac{U_x}{d_x} \gg \dfrac{Q_s^2}{16\pi\varepsilon_0}\left[\dfrac{1}{(d_{xn} - d_x)^2} - \dfrac{1}{d_x^2}\right] \end{cases} \tag{6}$$

Therefore, the electric image forces f_{ix} and f_{iy} are quite small, and they are neglected in the horizontal motion control of test sample in the electrostatic suspension system.

However, for the motion control of test sample in the vertical direction, the gravity of test sample causes it to deflect from the equilibrium position such that a great displacement deviation possibly occurs, so the electric image force f_{iz} must be considered in vertical motion control.

Based on the above analysis about test sample in the electrostatic suspension system, the equations of motion of test sample in vertical and horizontal directions could be expressed as

$$\begin{cases} m\ddot{d}_x = Q_s \dfrac{U_x}{d_x} \\ m\ddot{d}_y = Q_s \dfrac{U_y}{d_y} \\ m\ddot{d}_z = Q_s \dfrac{U_z}{d_z} + \dfrac{Q_s^2}{16\pi\varepsilon_0}\left[\dfrac{1}{(d_{zn}-d_z)^2} - \dfrac{1}{d_z^2}\right] - mg \end{cases} \tag{7}$$

where d_x is the airgap between the mass center of test sample and the HV electrode in x axis, d_y is the airgap between the mass center of test sample and the HV electrode in y axis. In the meanwhile, the accelerations in horizontal and vertical directions could be defined as

$$a_x = \ddot{d}_x, \quad a_y = \ddot{d}_y, \quad a_z = \ddot{d}_z \tag{8}$$

The vertical suspension control of test sample is chosen as the analysis example, and then the control voltages of vertical HV electrodes could be expressed as the terms of acceleration and displacement as following

$$U_z = \frac{ma_z d_z}{Q_s} - \frac{Q_s d_z}{16\pi\varepsilon_0}\left[\frac{1}{(d_{zn}-d_z)^2} - \frac{1}{d_z^2}\right] + \frac{mgd_z}{Q_s} \tag{9}$$

Therefore, the control loop of test sample in the electrostatic suspension system could be divided into the control loop of displacement and the control loop of acceleration. In order to ensure the test sample suspends stably at the equilibrium position on the ground experiment, the accelerations along horizontal and vertical directions are setting to zero.

2.3 Stable Suspension Conditions of Test Sample

As the important parts in force analysis of test sample in the electrostatic suspension system, and equivalent stable suspension conditions of electric field force would be analyzed. The charge of test sample is calculated by following equation [25]

$$Q_s = 4EK\pi\varepsilon_0 r^2 \tag{10}$$

where r is the radius of test sample, E is the electric field strength, and K is the influence coefficient of electrode shape for charge of test sample.

At the initial suspension position, the electric field force should be equal to the gravity of test sample, so there is

$$f_{ez} = \beta Q_s E = mg = \frac{4}{3}\pi r^3 \rho g \tag{11}$$

where β is the influence coefficient of electrode shape for the surface charge distribution of test sample, and ρ is the density of test sample.

Combining (10) and (11), the electric field strength and the charge of test sample should satisfy the following conditions to make the test sample stably suspend at the vertical equilibrium position,

$$\begin{cases} E = \sqrt{\dfrac{\rho g r}{3K\varepsilon_0\beta}} \\ Q_s = 4\pi\sqrt{\dfrac{\rho g K\varepsilon_0 r^5}{3\beta}} \end{cases} \tag{12}$$

And then the electric image force of test sample at initial suspension position is

$$(1-\beta)Q_s E = \frac{Q_s^2}{16\pi\varepsilon_0 d^2} \tag{13}$$

The minimum airgap in vertical direction is

$$d = \sqrt{\frac{Kr^2}{4(1-\beta)}} \tag{14}$$

Therefore, the electric image force f_{iz} decreases with the airgap between the center of mass and the below electrode in vertical direction. In addition, the charge of test sample at the equilibrium position would be quickly declined during the heating process, and then the electric field force will change rapidly with the varying charge of test sample. Moreover, the vibration and deflection of HV electrodes also affect the stable suspension status of test sample. Consequently, the test sample in the electrostatic suspension system is not self-sable, a closed-loop control system is needed to guarantee the stable suspension of test sample in the electrostatic suspension system.

3 Control Scheme Design of Electrostatic Suspension System

For the test sample in the electrostatic suspension system, the motion control along horizontal and vertical directions (x, y and z axis) are regarded as decoupled state. Therefore, the control loop of vertical suspension would be designed as like that in horizontal motion. In addition, since that the vertical motion of test sample is more complex than the horizontal motion considering the electric image force f_{iz} and the gravity mg in the vertical direction, the control loop of vertical motion is chosen as the example in following design, simulation and experiment.

3.1 ADRC Model of Electrostatic Suspension System

The ADRC model for the vertical motion of test sample is illustrated in Fig. 3, and it consists of three parts including the tracking differentiator (TD), the extended state observer (ESO) and the linear state error feedback (LSEF) control model. The TD could reconcile the contradiction between the fast response speed and the great overshoot by transferring the reference input into the gradual variable input. For the purpose of position control and vibration control for test sample, the whole control scheme has two control loops with a

displacement control loop in blue block diagram and an acceleration control loop in red block diagram. To realize the stable suspension of test sample without vibration, the reference input of acceleration control loop is set to zero on the ground experiments in this article.

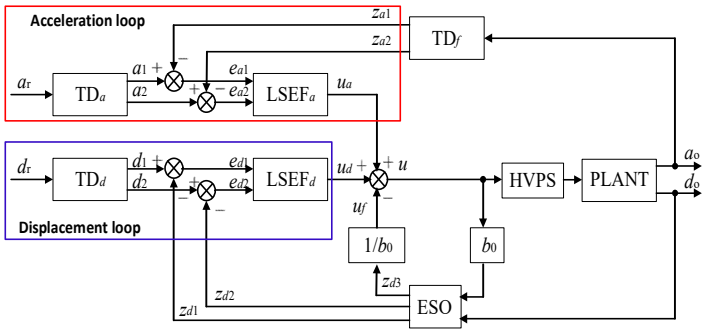

Fig. 3. The control scheme of test sample in the electrostatic suspension system.

3.2 *The Displacement Control Loop of Test Sample*

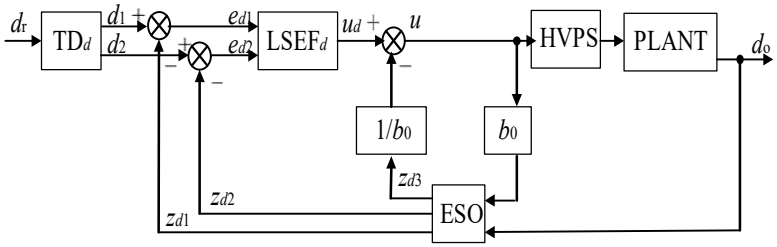

Fig. 4. The displacement control loop of test sample in the electrostatic suspension system.

For the displacement control loop of test sample in the electrostatic suspension system in Fig. 4, the reference displacement signal d_r is converted into the displacement control signal d_1 and the displacement differential signal d_2 through the displacement tracking differentiator TD_d. The ESO could achieve the observed value of output displacement z_{d1}, the observed value of velocity z_{d2} and the observed value of system disturbance z_{d3}. Furthermore, the displacement error e_{d1} and the velocity error e_{d2} are transformed into the displacement control signal u_d by the LSEF_d in the displacement control loop.

For the displacement control loop shown in Fig. 4, the displacement tracking differentiator TD_d is designed as

$$\begin{cases} \dot{d}_1 = d_2 \\ \dot{d}_2 = d_3 \\ \dot{d}_3 = -p_d\{p_d[p_d(d_1 - d_r) + 3d_2] + 3d_3\} \end{cases} \tag{15}$$

where p_d is the control parameter of displacement tracking differentiator TD_d.

The ESO not only observes the system sates of electrostatic suspension system, but also observes the system disturbance including the disturbance terms and the parameter uncertainty. Therefore, an extra state observation is added to observe the 'total' disturbances, and ESO is designed as following

$$\begin{cases} e = z_{d1} - d_o \\ \dot{z}_{d1} = z_{d2} - \beta_1 e \\ \dot{z}_{d2} = z_{d3} - \beta_2 e + b_0 u \\ \dot{z}_{d3} = -\beta_3 e \end{cases} \tag{16}$$

where b_0 is the gain of control voltage, $\beta_{i=1,2,3}$ are the control coefficients of ESO, and they could be chosen as following

$$\begin{cases} \beta_1 = 3\omega_{eso} \\ \beta_2 = 3\omega_{eso}^2 \\ \beta_3 = \omega_{eso}^3 \end{cases} \tag{17}$$

where ω_{eso} is the bandwidth of ESO.

The model of $LSEF_d$ in displacement control loop is chosen as

$$\begin{cases} e_{d1} = d_1 - z_{d1} \\ e_{d2} = d_2 - z_{d2} \\ e_{d0} = \int_0^t e_{d1} d\tau \\ u_d = k_{pd} e_{d1} + k_{id} e_{d0} + k_{dd} e_{d2} \end{cases} \tag{18}$$

where k_{pd} is proportional coefficient of $LSEF_d$, k_{ia} is integral coefficient of $LSEF_d$, and k_{dd} is derivative coefficient of $LSEF_d$.

3.3 The Acceleration Control Loop of Test Sample

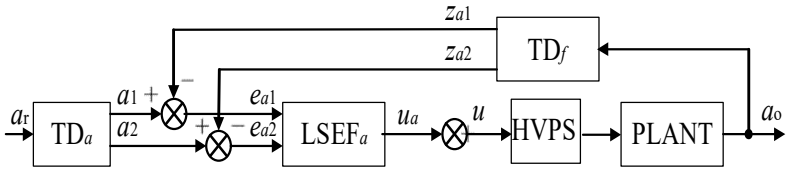

Fig. 5. The acceleration control loop of test sample in the electrostatic suspension system.

For the acceleration control loop of test sample in the electrostatic suspension system as illuminated in Fig. 5, besides an acceleration tracking differentiator TD_a, an feedback tracking differentiator TD_f in the feedback loop could get the micro gravity signal of test sample. The tracking differentiator TD_a is designed as following

$$\begin{cases} \dot{a}_1 = a_2 \\ \dot{a}_2 = a_3 \\ \dot{a}_3 = -p_a\{p_a[p_a(a_1 - a_r) + 3a_2] + 3a_3\} \end{cases} \tag{19}$$

where p_a is the coefficient of TD_a, and the feedback tracking differentiator TD_f is

$$\begin{cases} \dot{z}_{a1} = z_{a2} \\ \dot{z}_{a2} = z_{a3} \\ \dot{z}_{a3} = -p_f\{p_f[p_f(z_{a1} - a_o) + 3z_{a2}] + 3z_{a3}\} \end{cases} \tag{20}$$

where p_f is the coefficient of TD_f.

The model of $LSEF_a$ in acceleration control loop is

$$\begin{cases} e_{a1} = a_1 - z_{a1} \\ e_{a2} = a_2 - z_{a2} \\ u_a = k_{pa} e_{a1} + k_{da} e_{a2} \end{cases} \tag{21}$$

where k_{pa} is proportional coefficient of LSEF$_a$, and k_{da} is derivative coefficient of LSEF$_a$.

The compensation function for disturbance in the ESO is

$$u_f = -\frac{1}{b_0} z_{d3} \tag{22}$$

Therefore, the synthesized control signal of electrostatic suspension system is

$$u = u_a + u_d + u_f \tag{23}$$

Finally, the control output is amplified by the HVA and the HVPS to drive the HV electrodes generate electric field forces, and then control the stable suspension of test sample in the electrostatic suspension system, and the amplification coefficient k_a of the HVPS is 3000 in the vertical motion control.

4 Simulation

In the simulation part, the suspension traces of test sample with different control models are compared, and the overshoot and the settling time are used to evaluate the control performances of electrostatic suspension system with different control methods.

4.1 Electric Field Force and Electric Image Force

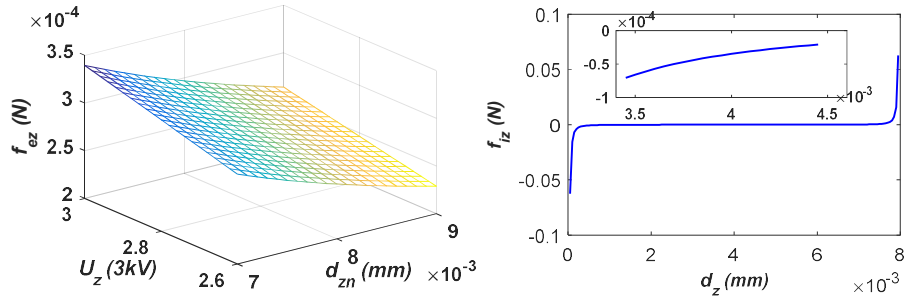

(a) (b)

Fig. 6. (a) The electric field force in vertical direction, (b) the electric image force in vertical direction.

In the electrostatic suspension system, the relationship among the electric field force f_{ez}, the airgap of vertical HV electrodes d_{zn} and the control voltage of vertical HV electrodes U_z are shown in Fig. 6(a), the electric field force is linear to the control voltage of vertical HV electrodes, and decreases with the airgap of vertical HV electrodes. In addition, the relationship between the electric image force f_{iz} and the displacement d_z of test sample is depicted in Fig. 6(b). The electric image force rapidly increases to a huge value when the test sample approaches to the top electrode or the below electrode in vertical direction. In the normal suspension range, the electric image force increases with the airgap between the test sample and the vertical HV electrode. Therefore, if there is no electric field force acting on the test sample, it will drop to the below electrode because of the gravity and the electric image force.

4.2 Suspension Precision of Test Sample

The initial position of test sample sets at 2.815mm in vertical direction, and then the suspension experiment of test sample is conducted. A step displacement signal shown by dotted line is used as the reference signal to make the test sample suspends at vertical equilibrium position in Fig. 7. The test sample is stably suspended at vertical equilibrium position when the displacement approaches to zero. For the suspension traces of test sample as illustrated in Fig. 7(a), and the settling time of suspension trace with PID model is 0.6s, and the overshoot is about 1.2mm. The suspension traces for the random disturbance with amplitude 0.05mm are plotted in Fig. 7(b), the root mean square (RMS) value of suspension trace with PID model is 0.1108mm, and that of the ADRC model is 0.0058mm.

When the test sample is stably suspended at the vertical equilibrium position, an impulse-type disturbance with 15% of test sample's gravity is imposed on it, and the response curves of test sample are plotted in Fig. 7(c). For the PID model, the settling time back to the equilibrium position is 0.3s, and the overshoot is 0.28mm. For the ADRC model, the settling time is shortened into 0.1s, but the overshoot increases to 0.32mm.

Therefore, as the comparison results listed in TABLE. I, the ADRC model for the electrostatic suspension system has a better performance on suppressing the disturbance by decreasing the settling time. Even though the overshoot amplitude would be intensified, the amplitude is still restrained in the stable region of electrostatic suspension system.

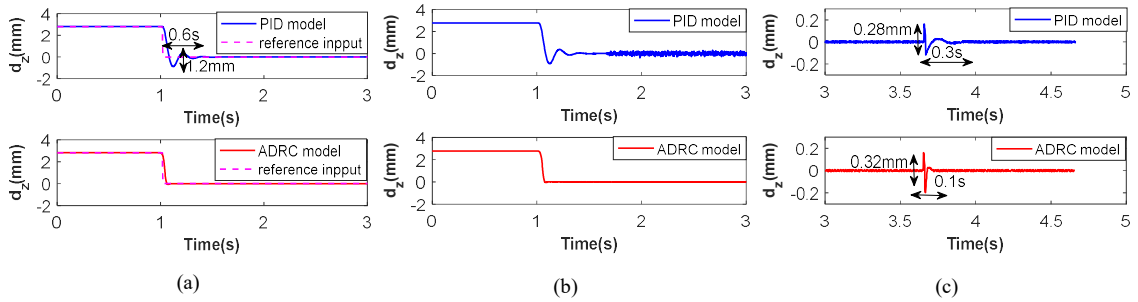

Fig. 7. Suspension traces of test sample in vertical direction, (a) static suspension in vertical direction, (b) suspension traces with random-type disturbance, (c) suspension traces with impulse-type disturbance.

TABLE. I. Performances of PID and ADRC models in simulation

	PID model			ADRC model		
	overshoot (mm)	settling time (s)	RMS (mm)	overshoot(mm)	settling time (s)	RMS (mm)
suspension traces	1.2	0.6		0.1	0.1	
random disturbance			0.1108			0.0058
Impulse disturbance	0.28	0.3		0.32	0.1	

4.3 Control Voltages of HV Electrodes

In addition, the curves of control voltage with different control models are plotted in Fig. 8, and the amplification coefficient of HVPS is 3000 in the control channel of vertical suspension. For the random disturbance, the control voltages of HV electrodes are depicted in Fig. 8(a), the overshoot of control voltage with PID model is smaller than that of the ADRC model, but the steady-state control voltage of the PID model

(RMS=0.0735) is obviously greater than the ADRC model (RMS=0.0235). In addition, for the response curve of impulse-type disturbance in Fig. 8(b), the overshoot of control voltage with PID model is about 1.99(×3000V), but that of the ADRC model is about 1.1(×3000V). Therefore, the ADRC model could suppress the overshoot in the control voltage when the electrostatic suspension system is suffered from the external disturbance.

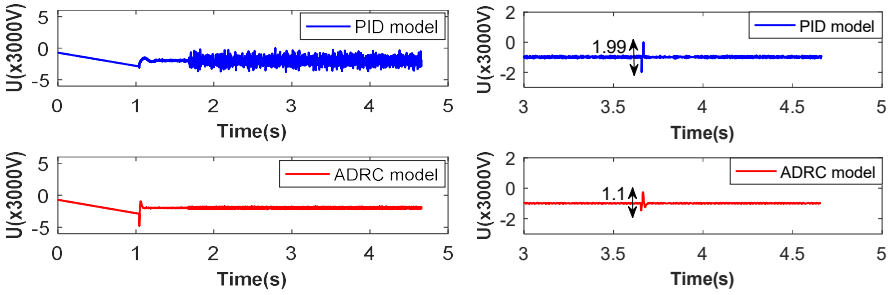

(a) (b)

Fig. 8. (a) The control outputs of PID and ADRC models for random-type disturbance, (b) the control outputs of PID and ADRC models for impulse-type disturbance.

4.4 Tracking Performance of Displacement Control Loop

The output terms of ESO with different disturbances in the displacement control loop of electrostatic suspension system are plotted in Fig. 9. For the random disturbance, the estimated value (RMS) of vertical displacement z_{d1} is 0.0057mm, and estimation error is 0.0178mm. Moreover, for the impulse disturbance, the overshoot value of vertical displacement z_{d1} is 0.39mm, and estimation error is 0.07mm. Compared to vertical displacement in Fig. 7(c), the relative error is about 17%. Therefore, the simulation result indicates that ESO could accurately estimate the displacement feedback terms z_{d1} and z_{d2} in vertical direction.

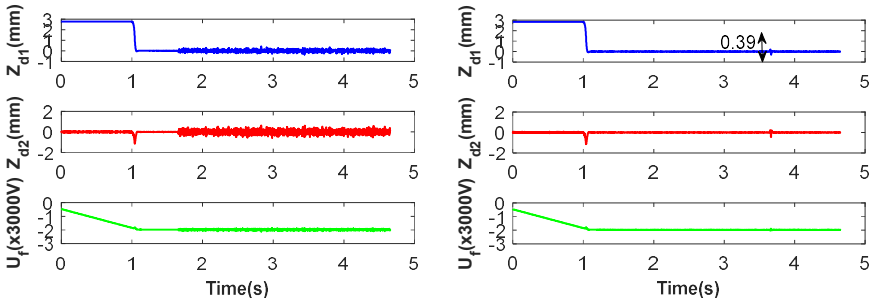

(a) (b)

Fig. 9. (a) The ESO outputs for a random-type disturbance, (b) the ESO outputs for an impulse-type disturbance.

5 Experiment

5.1 Experimental Setup

The experimental setup of electrostatic suspension system is illustrated in Fig. 10. The whole electrostatic suspension system is placed in a sealed container to minimize disturbances from external environment. The test sample and three pairs of HV electrodes are in the center of sealed container. The two

pairs of cameras are formed into the binocular vision system to measure the displacement variation of test sample, and then the displacement signals are feedbacked to the MCU based on SoC chip and GPU chip. The control signals are generated by the MCU, and the control voltages of HV electrodes would be regulated to realize the active suspension control of test sample through the HVPS. The silicon carbide ball is chosen as the test sample in the suspension experiment. Those relative parameters of the electrostatic suspension system are listed in TABLE. II.

The control parameters (p_d, p_a and p_f) in the tracking differentiators TD_d, TD_a and TD_f are used to generate the transition signals of acceleration and displacement, and the control parameters p_d, p_a and p_f could not cause serious influences to the static and dynamic characteristics of test sample in the electrostatic suspension system. Moreover, the parameter setting about p_d, p_a and p_f could be referred to the PD control model. According to the procedures of parameter tuning about the LSEF in Fig. 11, the control parameters of ADRC model are listed in TABLE. III.

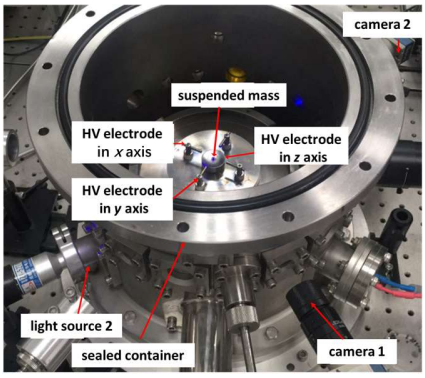

Fig. 10. The electrostatic suspension system.

Step1: chosen the bandwidth of ESO ω_{eso}
Criterion: the bandwidth increases with disturbance frequency, but a large bandwidth would make output has fluctuation for low-frequency disturbance.

Step2: chosen the gain of control voltage b_0
Criterion: the great gain of control voltage could suppress the fluctuation caused by the bandwidth of ESO but would decrease the compensation term for disturbance.

Step3: chosen proportional coefficient k_{pd} and derivative coefficient k_{dd} of $LSEF_d$
Criterion: with certain values ω_{eso} and b_0, the great values of proportional coefficient and derivative coefficient of $LSEF_d$ would make the output fluctuate.

Fig. 11. Parameter tuning of ADRC model in electrostatic suspension system.

TABLE. II. Parameters of electrostatic suspension system

Symbol	Quantity	Value
d_z	minimum airgap of vertical HV electrode	1.69mm
d_{zn}	maximum airgap of vertical HV electrode	8mm
d_x	minimum airgap of horizontal HV electrode	2.64mm
d_{xn}	maximum airgap of horizontal HV electrode	30mm
	amplification of horizontal HV electrode	1000
	amplification of vertical HV electrode	3000
ε_0	permittivity of vacuum	$8.85\cdot10^{-12}C^2/(Nm^2)$
Q	charge of test sample	$2.64\cdot10^{-10}C$
r	radius of test sample	1.185mm
ρ	density of test sample	$3.2g/cm^3$
m	mass of test sample	0.0125g
K	coefficient of electrode shape for charge	1.64
β	coefficient of surface charge distribution	0.8

TABLE. III. PARAMETERS OF CONTROL SYSTEM

Symbol	Quantity	Value
p_d	control coefficient of TD_d	10
p_a	control coefficient of TD_a	10
p_f	control coefficient of TD_f	10
b_i	gain of control voltage	3000
β_1	control coefficient of ESO	350
β_2	control coefficient of ESO	92795
β_3	control coefficient of ESO	398241
k_{pd}	proportional coefficient of displacement loop	0.7
k_{id}	integral coefficient of displacement loop	0.04
k_{dd}	derivative coefficient of displacement loop	0.018
k_{pa}	proportional coefficient of acceleration loop	1.967
k_{da}	derivative coefficient of acceleration loop	0.021
ω_{eso}	bandwidth of ESO	10Hz
	simulation frequency	1000Hz
	control frequency	100Hz

5.2 *Suspension Trace of Test Sample in Vertical Direction*

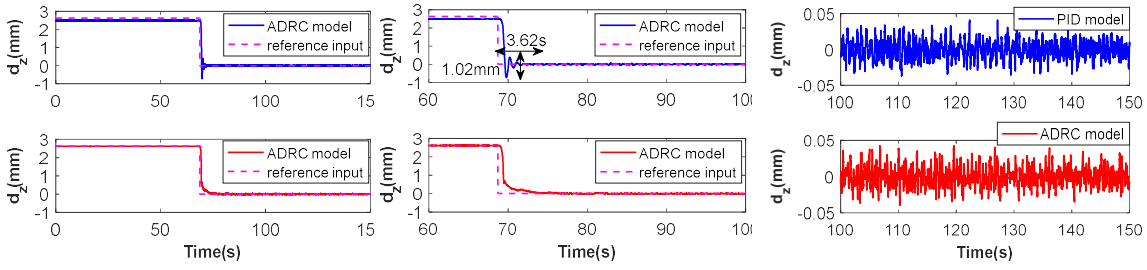

(a) (b) (c)

Fig. 12. (a) The suspension traces of test sample in vertical direction, (b) comparison of the overshoot and the settling time, (c) the steady-state suspension traces in vertical direction.

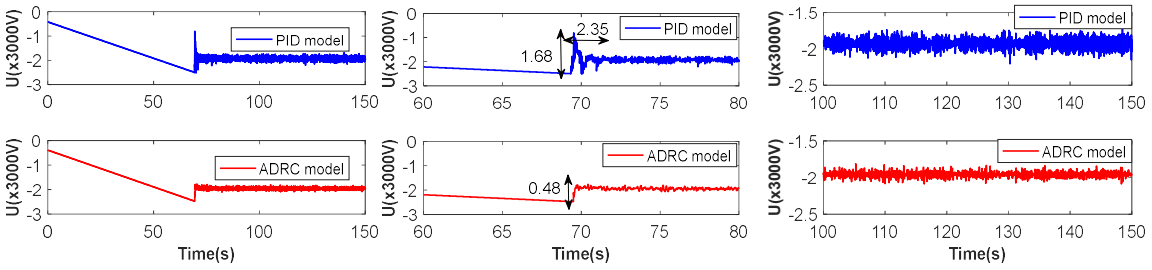

(a) (b) (c)

Fig. 13. (a) The control voltages during suspension process, (b) comparison of control voltages during suspension process, (c) control voltages during steady-state suspension.

In this part of experiment, the test sample (initial position is 2.815mm in vertical direction) is levitated to the equilibrium position by the electric field forces of HV electrodes in vertical direction. The suspension traces of test sample are plotted in Fig. 12(a) to compare control performances of different models, the blue line is the suspension trace of test sample with the PID model, and the red line presents the suspension trace of test sample with the ADRC model. This result indicates that the test sample could be suspended at the vertical equilibrium position with two control models. In addition, the settling time and overshoot of suspension traces are shown in Fig. 12(b). For the PID model, the settling time is about 3.62s, and the overshoot is 1.02mm. For

the ADRC model, the settling time and the overshoot are close to zero. Moreover, the steady-state suspension of test sample are plotted in Fig. 12(c), the root mean square (RMS) value is used to evaluate the steady-state suspension precision, and a smaller RMS value presents a higher steady-state suspension precision. The RMS value of PID model is 0.0122mm, and that of ADRC model is 0.0109mm. This comparison result of suspension traces implies that the ADRC model could reduce the settling time and the overshoot during the suspension process of test sample in the electrostatic suspension system.

In the meanwhile, the control voltages of HV electrodes are displayed in Fig. 13(a) during the vertical suspension process of test sample. For the PID model, the overshoot is about 1.68(×3000V), and the settling time is 2.35s as shown in Fig. 13(b). For the ADRC model, the overshoot is 0.48(×3000V). Furthermore, as shown in Fig. 13(c), for the control voltages during the steady-state suspension of test sample, the RMS of PID model is 0.0912(×3000V), and that of ADRC model is 0.0571(×3000V)

As similar as the suspension traces in vertical direction, the ADRC model could reduce the overshoot and the settling time of control voltages during the suspension process, and the steady-state precision of control voltage is improved about 76%. Therefore, the ADRC model would cause less influence on the HVPS than the PID model, and then the reliability of electrostatic suspension system is enhanced.

5.3 Tracking Performance of Test Sample in Vertical Direction

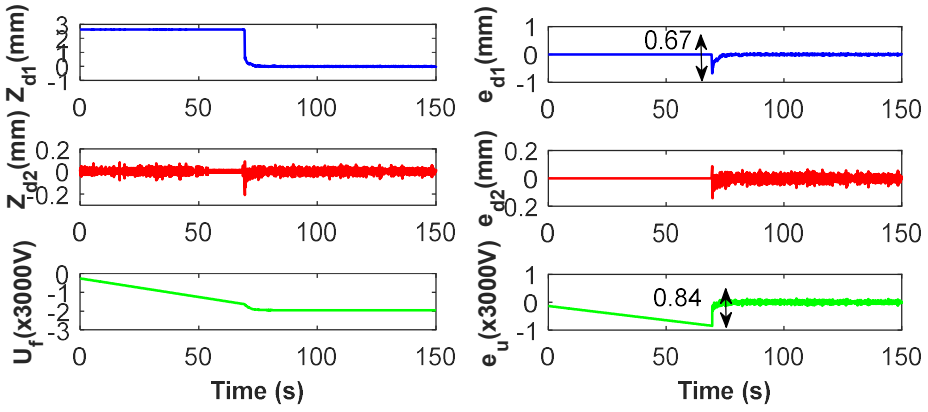

(a) (b)

Fig. 14. (a) The ESO output during suspension process in vertical direction, (b) the error between estimated value and real value.

The ESO outputs are also recorded in this suspension experiment to evaluate the tracking performance of the ADRC model. As shown in Fig. 14(a), the first figure is the estimated value of test sample's displacement in vertical direction, and the errors between the estimated value and the reference input are plotted in Fig. 14(b). The maximum error 0.67mm occurs at the initial suspension position, and the steady-state error is about 0.0142mm as shown in first figure in Fig. 14(a). The middle figure in Fig. 14(a) is the estimated value of differential signal of vertical displacement, and it is always kept at the balanced status before the test sample is levitated to the equilibrium suspension position. The below figure in Fig. 14(a) shows the estimated value of control voltage, and the estimated value has good tracking performance for the reference control voltage. The error curve between the estimated value and the real value of control voltage is shown in the below figure of

Fig. 14(b), the maximum error is 0.84(×3000V) at the initial suspension position, and the error of control voltage during the steady-state suspension is 0.0339(×3000V). Therefore, the ESO could accurately track the displacement and control voltage of the electrostatic suspension system.

5.4 Disturbance Rejection Performance of Test Sample in Vertical Direction

When an impulse-type disturbance (amplitude is 15% of test sample's gravity) is imposed on the test sample at the equilibrium suspension position, the suspension traces of test sample are plotted in Fig. 15(a). For the PID model, the overshoot of suspension trace is 1.54mm and the settling time back to the equilibrium suspension position is 1.26s. Moreover, for the ADRC model, the overshoot is 1.11mm with the settling time 0.59s. The control voltages for the impulse-type disturbance are measured and plotted in Fig. 15(b). The overshoot value of control voltage with PID model is 2.63(×3000V), and that of the ADRC model is 1.84(×3000V), so the relative reduction is 30%.

Therefore, as listed in TABLE. IV, the comparisons about suspension traces and control voltages for the impulse-type disturbance indicate that the ADRC model could quickly force the test sample back to the equilibrium suspension position with small overshoot and short settling time. In the meanwhile, the control voltages of HV electrodes are controlled well with small oscillation and pulse.

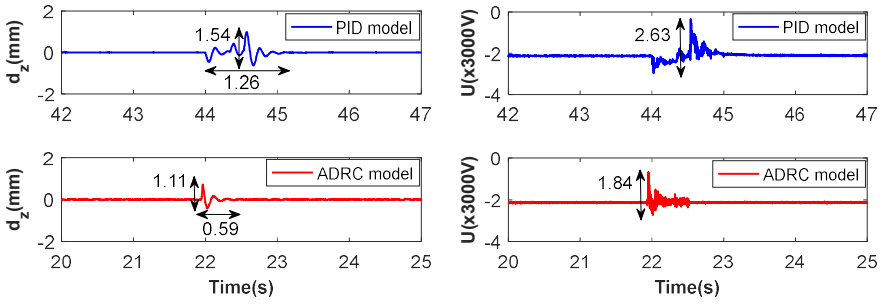

Fig. 15. (a) The suspension traces with impulse-type disturbance, (b) the control voltages of HV electrodes for impulse-type disturbance.

TABLE. IV. Performances of PID and ADRC models in experiment

	PID model			ADRC model		
	overshoot (mm)	settling time (s)	RMS (mm)	overshoot (mm)	settling time (s)	RMS (mm)
suspension trace	3.62	1.02	0.0122	0.1	0.1	0.0109
impulse disturbance	1.54	1.26		1.11	0.59	

6 Conclusion

The vertical motion control of test sample in the electrostatic suspension system is easily affected by the gravity, the variable electric image force and the external disturbances acting on the HV electrodes. Therefore, the ADRC model combining with a displacement control loop and an acceleration control loop is designed for the suspension control of test sample in the electrostatic suspension system. When the random and impulse disturbances are imposed on the test sample, the simulation and experimental results indicate that the ADRC model has good performance on disturbance attenuation by reducing the overshoot and the settling time.

Therefore, this research would be applied into the material testing using the electrostatic suspension system to improve the suspension stability of test sample and reduce impact on the HV electrodes.

References

[1] M.P. Sansoucie, J.R. Rogers, T. Tramel, Electrostatic Levitation for Studies of Additive Manufactured Materials, (2014).

[2] J. Liu, Q. Wang, X. Li, Design of hybrid suspension system of superconducting and electrostatic suspension, IEEE Transactions on Applied Superconductivity, 21 (2010) 1502-1506.

[3] N.A. Mauro, W. Fu, J.C. Bendert, Y.Q. Cheng, K.F. Kelton, Local atomic structure in equilibrium and supercooled liquid Zr75.5Pd24.5, Journal of Chemical Physics, 137 (2012) 044501.

[4] D. Quirinale, G. Rustan, S. Wilson, M. Kramer, A. Goldman, M. Mendelev, Appearance of metastable B2 phase during solidification of Ni50Zr50 alloy: electrostatic levitation and molecular dynamics simulation studies, Journal of Physics: Condensed Matter, 27 (2015) 085004.

[5] D.G. Quirinale, G.E. Rustan, A. Kreyssig, A.I. Goldman, In Situ X-ray Diffraction Studies of Metastable Phase Formation in Fe83B17 using Electrostatic Levitation, in: APS March Meeting Abstracts, 2015.

[6] Y. Ohishi, H. Muta, K. Kurosaki, J.T. Okada, T. Ishikawa, Y. Watanabe, S. Yamanaka, Thermophysical properties of molten core materials: Zr–Fe alloys measured by electrostatic levitation, Journal of Nuclear Science and Technology, 53 (2016) 1943-1950.

[7] Y. Ohishi, T. Kondo, T. Ishikawa, J.T. Okada, Y. Watanabe, H. Muta, K. Kurosaki, S. Yamanaka, Physical properties of molten core materials: Zr-Ni and Zr-Cr alloys measured by electrostatic levitation, Journal of Nuclear Materials, 485 (2017) 129-136.

[8] P.-F. Paradis, T. Ishikawa, G.-W. Lee, D. Holland-Moritz, J. Brillo, W.-K. Rhim, J.T. Okada, Materials properties measurements and particle beam interactions studies using electrostatic levitation, Materials Science and Engineering: R: Reports, 76 (2014) 1-53.

[9] P. Lü, K. Zhou, H. Wang, Evidence for the transition from primary to peritectic phase growth during solidification of undercooled Ni-Zr alloy levitated by electromagnetic field, Scientific reports, 6 (2016) 39042.

[10] M. Beaudhuin, K. Zaidat, T. Duffar, M. Lemiti, Silicon purity controlled under electromagnetic levitation (SPYCE): influences on undercooling, Journal of materials science, 45 (2010) 2218-2222.

[11] M. Zhang, Y. Liu, J. Yu, X. Pan, S. Yoda, A novel upconversion TiO2–La2O3–Ta2O5 bulk glass co-doped with Er3+/Yb3+ fabricated by containerless processing, Materials Letters, 66 (2012) 367-369.

[12] S. Tsujino, T. Tomizaki, Ultrasonic acoustic levitation for fast frame rate X-ray protein crystallography at room temperature, Scientific reports, 6 (2016) 25558.

[13] T. Ishikawa, P.-F. Paradis, Challenges of handling, processing, and studying liquid and supercooled materials at temperatures above 3000 K with electrostatic levitation, Crystals, 7 (2017) 309.

[14] T. Le, J. Jeon, S. Woo, T. Higuchi, An electrostatic suspension system using piezoelectric actuators, Smart Materials and Structures, 21 (2012) 025012.

[15] T. Nakamura, Y. Awa, H. Shimoji, H. Karasawa, Control system of electrostatic levitation furnace, Acta Astronautica, 50 (2002) 609-614.
[16] J.U. Jeon, Time delay effects on performance and stability of a low cost electrostatic suspension system, International Journal of Precision Engineering and Manufacturing, 11 (2010) 549-557.
[17] T. Le, J. Jeon, Stability analysis of a time-optimally controlled electrostatic suspension system and suspension experiments in a vacuum, Proceedings of the Institution of Mechanical Engineers, Part C: Journal of Mechanical Engineering Science, 225 (2011) 88-100.
[18] L. Hu, H. Wang, W. Xie, B. Wei, Electrostatic levitation under the single-axis feedback control condition, Science China Physics, Mechanics and Astronomy, 53 (2010) 1438-1444.
[19] T. Meister, H. Werner, G. Lohoefer, D. Herlach, H. Unbehauen, Gain-scheduled control of an electrostatic levitator, Control Engineering Practice, 11 (2003) 117-128.
[20] Q.J. Xiao, S.-Y. Li, W.-Y. Chen, F. Cui, W.-P. Zhang, Fuzzy tuning PI control for initial levitation of micromachined electrostatically levitated gyroscope, Electronics Letters, 45 818.
[21] J. Han, From PID to Active Disturbance Rejection Control, IEEE Transactions on Industrial Electronics, 56 (2009) 900-906.
[22] R. Madonski, M. Ramirez-Neria, M. Stanković, S. Shao, Z. Gao, J. Yang, S. Li, On vibration suppression and trajectory tracking in largely uncertain torsional system: An error-based ADRC approach, Mechanical Systems and Signal Processing, 134 (2019) 106300.
[23] Z. Cai, J. Lou, J. Zhao, K. Wu, N. Liu, Y.X. Wang, Quadrotor trajectory tracking and obstacle avoidance by chaotic grey wolf optimization-based active disturbance rejection control, Mechanical Systems and Signal Processing, 128 (2019) 636-654.
[24] C. Aguilar-Ibañez, H. Sira-Ramirez, J.Á. Acosta, Stability of active disturbance rejection control for uncertain systems: A Lyapunov perspective, International Journal of Robust and Nonlinear Control, 27 (2017) 4541-4553.
[25] Colver, G. M., Dynamic and stationary charging of heavy metallic and dielectric particles against a conducting wall in the presence of a dc applied electric field, Journal of Applied Physics, 47 4839.